11th International Symposium on Turbulence and Shear Flow Phenomena (TSFP11)
Southampton, UK, July 30 to August 2, 2019

LEADING EDGE VORTEX FORMATION AND DETACHMENT ON A FLAT PLATE UNDERGOING SIMULTANEOUS PITCHING AND PLUNGING MOTION: EXPERIMENTAL AND COMPUTATIONAL STUDY

Johannes Kissing, Sebastian Wegt, Suad Jakirlic and Cameron Tropea
Institute of Fluid Mechanics and Aerodynamics, Technische Universität Darmstadt
Alarich-Weiss-Straße 10, 64287 Darmstadt, Germany
kissing, wegt, jakirlic, ctropea@sla.tu-darmstadt.de

Zhenyao Li and Lihao Feng
Institute of Fluid Mechanics, Beihang University
No. 37 Xueyuan Road, Haidian District, Beijing, P.R. China, 100083
lizhenyao1992@qq.com, lhfeng@buaa.edu.cn

ABSTRACT

The formation and detachment of a leading edge vortex (LEV)appearing on an airfoil when its effective angle of attack is dynamically changed, induces additional forces and moments on the airfoil. While the increased lift during the LEV growth can be advantageous for certain applications, e.g. on micro air vehicles (MAVs), on other applications, such as helicopter blades or wind turbine blades under gusty conditions, the detrimental pitching moment during the LEV detachment can endanger the structural integrity if components. These latter situations motivated the present work dealing with a complementary experimental and computational investigation of the flow past a pitching-plunging flat plate. The experimental study captures the time-resolved velocity field around the moving airfoil using PIV (particle image velocimetry). In the computational part an unsteady RANS (Reynolds-Averaged Navier-Stokes) framework employs a transition-sensitive Reynolds-stress model of turbulence proposed by Maduta *et al.* (2018), which combines the Reynolds-Stress model by Jakirlic *et al.* (2002) and a phenomenological transition model governing the pre-turbulent kinetic energy by Walters & Cokljat (2008). The study focusses on the leading edge vortex formation and its development, characterized by highly dynamic processes of mass and circulation transfer from the separated shear layer that ultimately determines the size and circulation of the LEV, up to its detachment from the airfoil. The present study deals with the one-shot downstroke motion of a generic flat plate at dimensionless numbers representative of efficient forward flight. Combined pitching and plunging kinematics enable the effective on-flow angle to be set arbitrarily.
Qualitative comparison of the flow fields and quantitative comparison of the LEV circulation and position, with the aid of vortex identification methods, show that computations successfully capture the vortex growth phase and its detachment.

INTRODUCTION

Aerodynamic forces and moments induced by the leading edge vortex (LEV) on airfoils that experience a sudden change in angle of attack are of relevance for a multitude of applications. The induced lift during the growth phase of the LEV is exploited by insects to attain higher lift and is often considered as a role model for the development of propulsion concepts for Micro Air Vehicles (MAVs). However, in other applications the negative pitching moment on the airfoil during the LEV detachment can endanger the structural integrity of components, for example rotating helicopter blades or wind turbine blades.
Topological flow characteristics on an airfoil experiencing a dynamic change of the on-flow angle are described by the dynamic stall phenomena (McCroskey (1982) and Carr (1988)). With an increasing angle of attack the flow over the airfoil separates and recirculates increasingly earlier until the boundary layer at the leading edge starts to roll up into a LEV. When the angle of attack is further increased, the vortex grows by accumulating mass and circulation transferred from the separated leading edge shear layer. As long as the vortex is attached to the airfoil, the dynamic lift significantly exceeds the static lift. Dependent on the experimental parameters, flow reversal at the trailing edge or an eruption of the boundary layer beneath the vortex lead to vortex detachment (Widmann & Tropea (2015)). Both mechanisms have in common that secondary structures growing above the airfoil surface, ahead of the main vortex and cut off the LEV from its feeding shear layer. Due to the convection of circulation, the dynamic lift is significantly lower than the static lift during and after the detachment phase of the vortex according to Wu *et al.* (2006). Additionally, a negative pitching moment is induced on the airfoil.
The overall scope of the current project is to increase the dynamic lift by delaying the leading edge vortex detachment experimentally with the aid of a dielectric barrier discharge (DBD) plasma actuator. Preliminary numerical studies are intended to identify topologically effective and

efficient actuation strategies in terms of actuation strength, timing and location. Therefore a common numerical and experimental baseline case of the unactuated flow field around a pitching and plunging flat plate airfoil is used to validate the numerical setup and this baseline case is the topic of the present study. Subsequently, based on a valid numerical representation of the unactuated flow field, the DBD plasma actuator will be introduced in future studies.

AIRFOIL AND MOTION KINEMATICS

A flat plate airfoil of 120 mm chord and 6 mm thickness with an asymmetric, sharp leading and trailing edge of 30° tip angle, as shown in Fig. 1, is chosen as a generic flow configuration. The sharp leading edge geometry is intended to produce a distinct shear layer separation that allows stable vortices to emerge during the airfoil motion. As an ex-

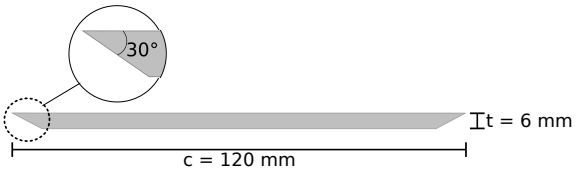

Figure 1: Flat plate airfoil of 5% thickness with a sharp leading edge (30° tip angle).

tract from cyclic motion, i.e. sinusoidal, one-shot, downstroke kinematics with combined pitching and plunging motion, is investigated. By adding pitching motion to pure plunging motion, the effective angle of attack of the on-flow on the flat plate $\alpha_{eff,PitchPlunge}(t)$ can be adjusted by adding a geometric angle of attack $\alpha_{geo,PitchPlunge}(t)$ to the angle of attack induced by the plunging motion $\alpha_{eff,Plunge}(t)$.
The computational study follows closely the experimental conditions; accordingly, the effective angle of attack history was chosen to be quasi-sinusoidal with 30° amplitude to generate a sinusoidal $\alpha_{geo,PitchPlunge}(t)$ evolution according to Eq. (1):

$$\alpha_{geo,PitchPlunge}(t) = 30° sin(\frac{\pi t}{T}) \qquad (1)$$

To investigate a flow configuration representative of biological propulsion in terms of dimensionless numbers, the chord based Reynolds number $Re = \frac{U_\infty c}{\nu}$,with the free stream velocity U_∞, the chord of the flat plate c and the kinematic viscosity ν, was set to 24000 (Anderson *et al.* (1998)). With the same intention, the reduced frequency $k = \frac{\pi c}{U_\infty T}$, with the motion period of the full cycle T, was set to 0.48 and the Strouhal Number $St = \frac{hc}{U_\infty T}$, with the stroke height $h = 0.15$ m. The corresponding evolution of effective and geometric angles of attack can be seen in Fig. 2.

EXPERIMENTAL SETUP

The experimental investigations were conducted in an open return wind tunnel at the Technische Universiät Darmstadt, with a test section of cross-section of 450 x 450 mm. The free stream turbulence level in the test section

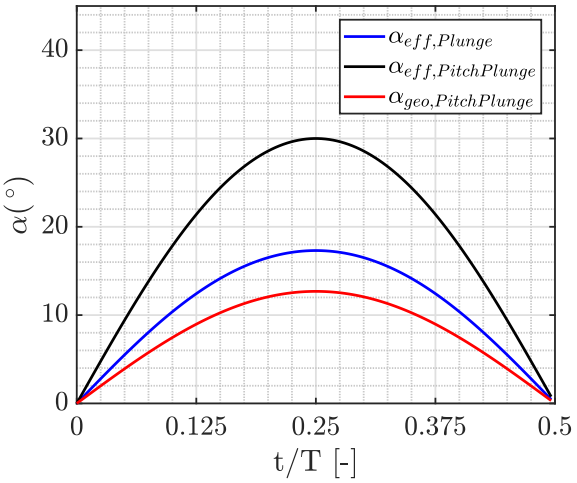

Figure 2: Evolution of the effective angle of attack $\alpha_{eff,PitchPlunge}$ introduced by the combined pitching and plunging motion of the airfoil. The geometric angle of attack $\alpha_{geo,PitchPlunge}$ is added to the induced angle of attack $\alpha_{eff,Plunge}$ to produced a distinct $\alpha_{eff,PitchPlunge}$ evolution for $Re = 24000$, $St = 0.1$ and $k = 0.48$.

T_u was measured to be below 0.3% for the investigated free stream velocity of $U_\infty = 3.335\,\mathrm{m\,s^{-1}}$. An encoder controlled pitch-plunge apparatus using magnetic driven shafts was used to move the airfoil that spanned the entire tunnel width to avoid three-dimensional flow effects. The maximum deviation of acceleration between the prescribed and measured value was always less than 7% for the investigated parameter range.
The flow field was measured using 2D2C time-resolved particle image velocimetry at an image pair acquisition frequency of 1000 Hz. A laser light sheet positioned at a quarter span of the airfoil with 2 mm thickness was produced by a frequency doubled, dual cavity Nd:YLF laser. A Photron© *SA1.1* CMOS camera with a resolution of 1024 x 1024 pixels captured the DEHS seeded flow in a field of view spanning $x/c = 1.2$ in the flow direction and $x/c = 1.2$ in the airfoil plunging direction. DEHS particles of about 1 µm size and a density of $900\,\mathrm{kg\,m^{-3}}$ were generated by blowing pressurized air through 4 Laskin nozzles into a seeding generator from which the aerosol was directed into the settling chamber of the wind tunnel through a seeding rake. Raw images were correlated using a multi-pass, multi-grid interrogation scheme with a final interrogation area (IA) size of 16 x 16 pixels and 50% overlap, providing a resolution of 1.3 mm/IA and 92 velocity information over the chord of the flat plate. A median based outlier filter with a threshold of 2 was used to exclude invalid vectors within a 3 x 3 neighbourhood after the final correlation. The maximum percentage of excluded velocity vectors was always below 3%. Excluded vectors were subsequently interpolated from their respective 3 x 3 neighbourhood.
In order to quantify the leading edge vortex circulation Γ_{LEV} and its center position (x_{LEV} and y_{LEV}), two scalar functions based on the method proposed by Graftieaux *et al.* (2001) were used. With the aid of the Γ_1 function the center of the vortex was identified while the Γ_2 scalar was used to obtain the vortex boundary by thresholding the scalar circulation field with $\Gamma_2 = 0.95$. To obtain Γ_{LEV},

the vorticity within the detected Γ_2 boundary was spatially integrated. For the investigated parameter set, 10 individual runs were recorded and correlated prior to the extraction of vortex quantities, which were then finally phase-averaged. For all investigated vortex quantities the standard deviation of the phase-averaged characteristics was found to be within 4 % of the asymptotic standard deviation computed from 30 runs.

COMPUTATIONAL METHOD, DETAILS

A differential Reynolds stress model (RSM) sensitive to transitional flow behavior was employed within the Unsteady RANS (Reynolds-Averaged Navier-Stokes) procedure. The modelling approach is based on blending the relevant source terms in the momentum and Reynolds stress equations with those originating from an appropriately modified eddy-viscosity based model governing the pre-turbulent kinetic energy. This model is designed to predict laminar-to-turbulent transition, rather than explicitly modifying the RSM equations in a term-by-term manner (see Maduta *et al.* (2018) for more details).
The model equations are implemented into the finite-volume-based open source toolbox OpenFOAM®, with which the present simulations are performed. The temporal resolution adopted yields a Courant number smaller than 1 over the entire solution domain. The discretization of the convective terms is performed by applying the well-known differed correction approach, blending appropriately between the Central Differencing (CDS) and the Upwind Scheme.
The flow domain is meshed using the OpenFOAM® code and its utility "blockMesh". A structured, fully hexahedral grid (Figure 3) consisting of 100,000 cells in the vertical plane is generated with a grading towards the plate and wind tunnel walls, providing the wall-next computational node situated well in the viscous sublayer with the dimensionless wall distance y^+ being substantially smaller than one for the entire simulation time. Accordingly, the governing equations are integrated to the wall, insuring that the near-wall region is fully resolved. The grid movement and deformation occurring during the pitching-plunging motion is accounted for by using the technique based on the radial basis function developed by Bos *et al.* (2013). The experimentally measured inflow velocity and turbulence are prescribed at the inflow plane situated at $0.985m$ in front of the flat-plate leading edge.

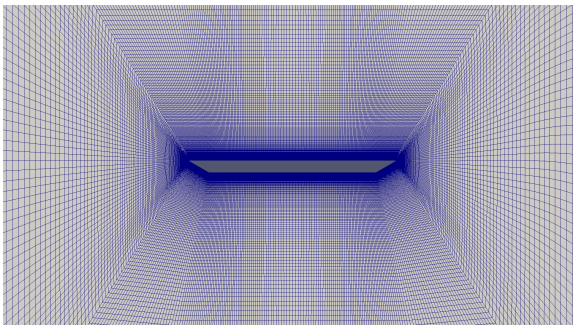

Figure 3: The numerical grid around the flat plate

RESULTS AND DISCUSSION

Phase-averaged experimental results of the flow field around the flat plate undergoing combined pitching and plunging downstroke motion in terms of normalized vorticity $\omega = \frac{\omega c}{U_\infty}$ are shown in figure 4 for different dimensionless time instants t/T. The on-flow is in the positive x-direction and the airfoil is translated in the negative y-direction. For $t/T = 0.125$ the vortex grows close to the leading edge, attached to the airfoil surface, with the rear flow reattachment point behind the vortex at about $x/c = 0.25$. At this early stage the vortex core consists of concentrated vorticity with a large gradient at its outer boundary. The normalized vorticity attains values of about -40 within the vortex core during this phase of the LEV growth. At $t/T = 0.25$ a counter-rotating secondary vortex arises on the airfoil surface between the vortex and the separated shear-layer at the leading edge. The rear reattachment point behind the vortex reaches the trailing edge at about $t/T = 0.375$, where the vortex center has passed half of the airfoils chord. At this instant the absolute dimensionless peak vorticity value has decreased to about -30. Subsequently, further growing secondary structures, in terms of the secondary and a tertiary vortex, ahead of the LEV can be observed that separate the vortex from its feeding shear layer at $t/T = 0.5$, where the vortex center has travelled downstream of the trailing edge. Fig. 5 illustrates the temporal evolution of the normalized vorticity field obtained from numerical simulations (Figure 5). At the first dimensionless time instant, a concentrated vortex core containing normalized vorticity with values around -40 and the stagnation point of the flow behind the vortex at about $x/c = 0.25$ are in close agreement with the experimental results. The thinner layer of opposite (positive) signed vorticity below the leading edge vortex on the airfoil surface can be attributed to the increased spatial resolution of the numerical results. At $t/T = 0.25$ pronounced secondary structures ahead of the main vortex can be observed, in agreement with experimental results at this instant. The dimensionless time instant at which the rear reattachment point behind the vortex has travelled downstream of the trailing edge ($t/T = 0.375$) is, analogously to the experimental flow fields, accompanied by growing secondary structures, that separate the LEV from the leading edge shear layer at $T/T0.5$. The absolute dimensionless vorticity peak value at $t/T = 0.375$ is with -30 comparable with experimental results at the same time instant.
To quantify the agreement between experiments and simulations in terms of leading edge vortex characteristics, its circulation Γ_{LEV} was obtained from velocity fields using the vortex identification method proposed by (Graftieaux *et al.*, 2001). Figure 6 shows the comparison of the time resolved normalized circulation of the LEV obtained by spatial integration of the vorticity within the area detected by the Γ_2 scalar field with a threshold of $\Gamma_2 = 0.95$. For the experimentally determined circulation evolution, vortex characteristics were extracted independently from single runs prior to phase averaging. The gray shaded area indicates the standard deviation from phase averaging in both directions for the experimental results. The computationally obtained normalized circulation evolution follows the experimental obtained circulation closely up to $t/T = 0.2$. For later non-dimensional time instants, the experimentally determined circulation is lower than the computationally obtained one, with an almost constant offset considering the inherent scatter of the experimental data. Inspection of single frame experimental vortex identification results reveals

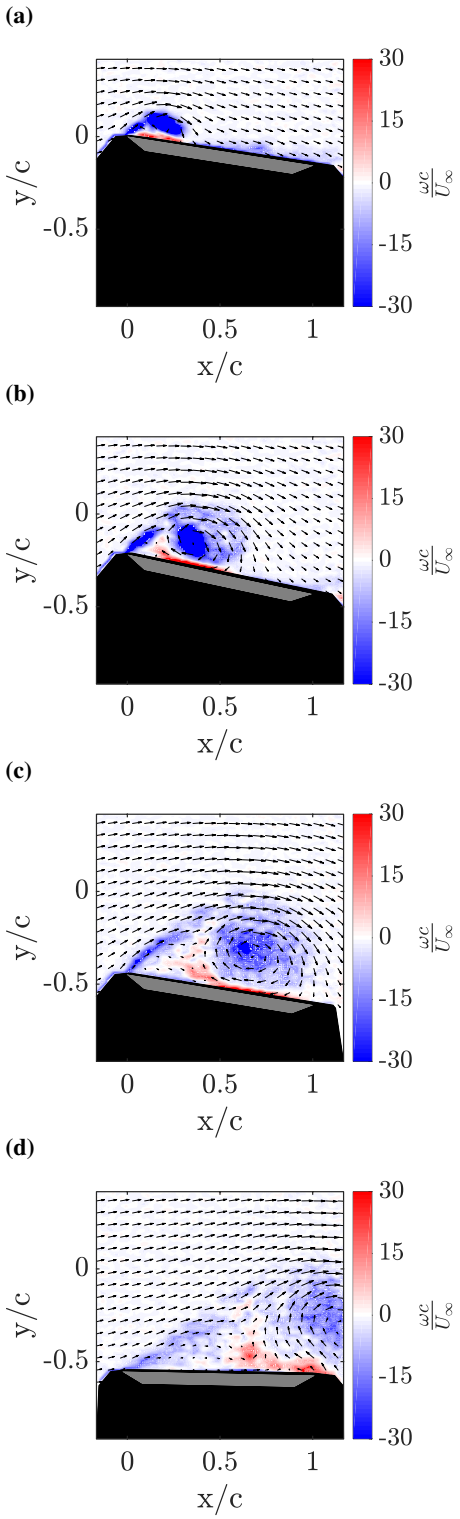

Figure 4: Time-resolved development of the normalized vorticity field $\frac{\omega c}{U_\infty}$ at $t/T = [0.125\ 0.25\ 0.375\ 0.5]$ for $Re = 24\,000$, $St = 0.1$ and $k = 0.48$ from PIV measurements.

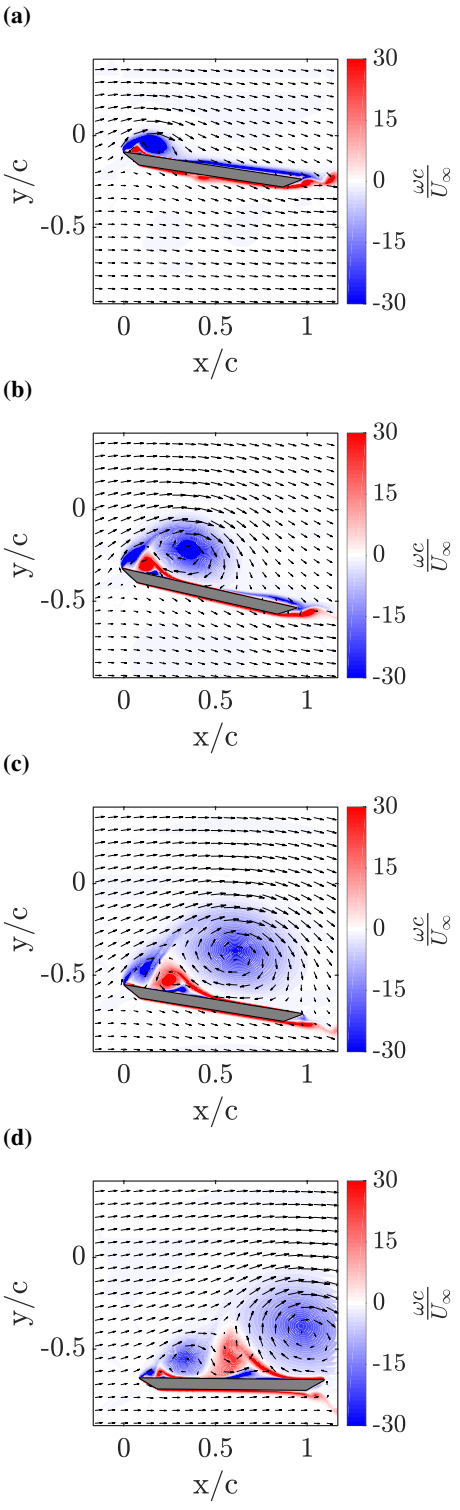

Figure 5: Temporal development of the normalized vorticity field ($\frac{\omega c}{U_\infty}$) obtained computationally. Key and scales as in Fig. 4.

that the drop in the experimentally obtained circulation evolution is caused by the fact that the leading edge shear layer is not contributing to the main vortex from $t/T = 0.2$ on. Based on this, the deviation of circulation evolution, encountered from $t/T = 0.2$ onward, can be attributed to the vortex identification approach used. The peak LEV circulation of both results was detected at about $t/T = 0.4$ with similar normalized circulation values, indicating good temporal and quantitative agreement between numerics and experiments regarding the LEV circulation evolution.

It is interesting to notice that the peak circulation occurs shortly after the rear reattachment point of the flow behind the vortex - a half saddle bound on the airfoil surface from a topological point of view - has travelled downstream of the trailing edge as observed in the flow fields. When this

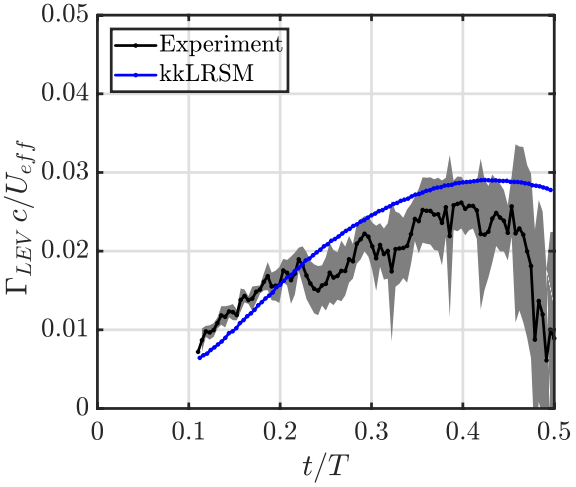

Figure 6: Comparison of the evolution of the normalized circulation of the vortex obtained by spatial integration of the vorticity within the area detected by the Γ_2 scalar field.

half saddle convects downstream beyond the trailing edge, fluid from below the airfoil can recirculate around the trailing edge and become entrained below the main vortex to finally be fed into the secondary vortex. The growing secondary vortex in turn can cut off the main LEV from the feeding shear layer, as observed by Rival *et al.* (2014) and thus, cause its detachment from the airfoil. In order to test this detachment hypothesis for the current experimental parameters, the velocity tangential to the airfoil surface, averaged over the first three velocity values above the airfoil is shown in figure 7.

The large negative (blue) diagonal areas in both diagrams are caused by the induced velocity of the clockwise rotating main LEV on the airfoil, which is against the on-flow direction. The white strip of zero velocity (marked with a green line) behind the LEV trace of negative velocity, indicates the location on the airfoil where the tangential velocity sign changes and thus the rear reattachment or half saddle of the flow behind the vortex. When the half saddle is convected downstream of the trailing edge at $x/c = 1$ (marked with an arrow), the above-mentioned detachment mechanism is initiated. The experimentally determined trace of the half saddle reaches the trailing edge at about $t/T = 0.36$ as shown in figure 7a, while the numerically obtained half saddle reaches the trailing edge at about $t/T = 0.38$. The time instant from which fluid can recirculate around the trailing edge occurs just before the corresponding peak LEV circulation is reached. This temporal sequence of fluid recirculation around the trailing edge and subsequent stop of circulation accumulation, in combination with growing secondary vortices, suggest a vortex detachment in accordance with the observations by (Rival *et al.*, 2014) for both investigations. Additionally the experimentally observed detachment mechanism is reproduced by computations.

In order to assess the vortex center convection parallel to the airfoil, which also determines the lift force exert by the LEV on the airfoil according to Wu *et al.* (2006), the vortex center was computed time-resolved from the velocity field using the Γ_1 criterion. Again, center locations were processed for individual experimental runs prior to phase-averaging. Figure 8 shows the comparison of numerically

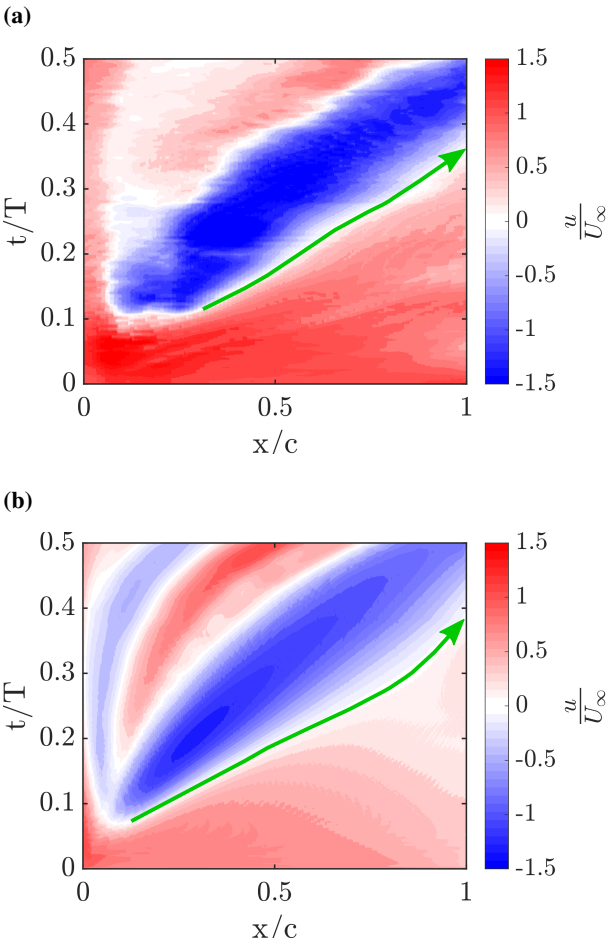

Figure 7: Evolution of the velocity tangential to the airfoil surface normalized by U_∞. The trace of the half saddle behind the LEV is marked with a green line and the time instant of recirculation around the trailing edge with an arrow. (a) Experimental tangential velocity; (b) Numerical tangential velocity.

and experimentally obtained vortex center locations, where the gray shaded area indicates the standard deviation of experimental phase averaging.

Up to $t/T = 3.3$ both center locations evolve in close agreement, whereas afterwards an increasing divergence of x_{LEV} up to 17% at $t/T = 0.45$ can be observed. Since the vortex was found to detach from its feeding shear layer due to recirculation of fluid around the trailing edge from $t/T = 0.375$ on, the deviation of its center position occurs at time instants that are no longer in focus for this study or for the overall project. A potential explanation of the deviation is the sensitivity of the vortex topology to small deviations early in the downstroke. Up to $t/T = 0.375$ the deviation of the LEV center position was found to be below 10%, which is considered as acceptable agreement.

CONCLUSIONS

Comparative numerical and experimental investigations of the leading edge vortex formation and detachment on a pitching and plunging flat plate have shown that computations successfully capture the vortex growth and de-

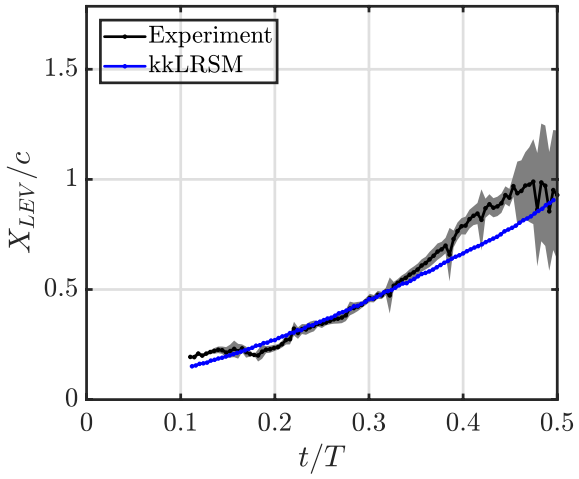

Figure 8: Comparison of the evolution of the vortex center x-location detected by the Γ_1 criterion. Frame of reference is parallel to the airfoil surface, with its origin at the moving leading edge.

tachment obtained from time-resolved particle image velocimetry. Topological flow features in terms of the LEV size and position, as well as the reattachment point of the flow behind the vortex on the airfoil surface and the evolution of secondary structures ahead of the main vortex are in close agreement.

A quantitative assessment of the time resolved LEV circulation and center position evolution with the aid of vortex identification methods has shown that numerical results coincide with experimentally obtained characteristics up to the detachment of the LEV. The vortex peak circulation value and instant, as well as its center position, could be reproduced numerically.

The LEV was found to stop accumulating circulation after the rear reattachment point of the flow behind the vortex has travelled downstream of the trailing edge. This suggests that for the investigated experimental conditions, a recirculation of fluid around the trailing edge initiates the growth of secondary structures that finally cut off the LEV from its feeding shear layer, as reported by (Rival *et al.*, 2014). This vortex detachment mechanism is common to both, experimental and numerical investigations.

OUTLOOK

Future numerical and experimental investigations concerning the LEV development on a NACA 0012 airfoil and experimental force measurements are intended to provide a wider base of comparison in terms of airfoil shapes and the lift coefficient. These will finally enable the application of the DBD plasma actuator numerically and experimentally, with the goal of prolonging the LEV growth phase; hence, attaining a stronger dynamic lift.

Acknowledgements. The financial support of the German Research Foundation (DFG) (Grant number TR 194/55-1) and Sino-German Center (Grant number GZ 1280) are gratefully acknowledged. The authors furthermore would like to thank the Lichtenberg HPC at TU Darmstadt for the computing time.

References

Anderson, J.M., Streitlien, K., Barrett, D.S. & Triantafyllou, M.S. 1998 Oscillating foils of high propulsive efficiency. *Journal of Fluid Mechanics* **360**, 41–72.

Bos, F.M., van Oudheusden, B.W. & Bijl, H. 2013 Radial basis function based mesh deformation applied to simulation of flow around flapping wings. *Computers and Fluids* **79**, 167–177.

Carr, L.W. 1988 Progress in analysis and prediction of dynamic stall. *Journal of Aircraft* **25** (1), 6–17.

Graftieaux, L., Michard, M. & Grosjean, N. 2001 Combining piv, pod and vortex identification algorithms for the study of unsteady turbulent swirling flows. *Measurement Science and Technology* **12** (9), 1422–1429.

Jakirlic, S., Hanjalic, K. & Tropea, C. 2002 Modeling rotating and swirling turbulent flows: A perpetual challenge. *AIAA Journal* **40** (10), 1984–1996.

Maduta, R., Wegt, S. & Jakirlic, S. 2018 A transition-sensitive Reynolds-stress model of turbulence. In *12th Int. ERCOFTAC Symp. on Engineering Turbulence Modelling and Measurements (ETMM12)*. Montpellier, France, September 26-28.

McCroskey, W.J. 1982 Unsteady airfoils. *Annual Review of Fluid Mechanics* **14** (1), 285–311.

Rival, D.E., Kriegseis, J., Schaub, P., Widmann, A. & Tropea, C. 2014 Characteristic length scales for vortex detachment on plunging profiles with varying leading-edge geometry. *Experiments in Fluids* **55** (1), 037,103.

Walters, D.K. & Cokljat, D. 2008 A three-equation eddy-viscosity model for reynolds-averaged navier–stokes simulations of transitional flow. *Journal of Fluids Engineering* **130** (12), 121401–14.

Widmann, A. & Tropea, C. 2015 Parameters influencing vortex growth and detachment on unsteady aerodynamic profiles. *Journal of Fluid Mechanics* **773**, 432–459.

Wu, J.-Z, Ma, H.-Y. & Zhou, M.-D. 2006 *Vorticity and Vortex Dynamics*. Berlin, Heidelberg: Springer Berlin Heidelberg.